

ScienceDirect



IFAC PapersOnLine 58-28 (2024) 672-677

A Transitional Intelligent Driver Model Enabling Vehicle Longitudinal Motion Prediction in Lane-Change Maneuvers

Sude E. Demir*, Xingyu Zhou*, Yanze Zhang†, Wenhao Luo†, and Junmin Wang*

* Walker Department of Mechanical Engineering, University of Texas at Austin Austin, TX 78712 USA

(e-mail: <u>sude.demir@utexas.edu</u>, <u>xingyu.zhou@austin.utexas.edu</u>, <u>jwang@austin.utexas.edu</u>)

† Department of Computer Science, University of North Carolina at Charlotte

Charlotte, NC 28223 USA

(e-mail: yzhang94@uncc.edu, wenhao.luo@uncc.edu)

Abstract: This paper proposes an extension of the Intelligent Driver Model (IDM) for predicting the vehicle longitudinal motion intentions during lane-changing maneuvers. The extension systematically creates a single, modified IDM model that can predict the ego vehicle's longitudinal motion with respect to both leading vehicles in the current and target lanes before, during, and after the lane change. A dynamic weighting function, determined by the ego vehicle's lateral displacement throughout the lane-changing maneuver, assigns relative importance to each of the two leading vehicles during integration. Several candidates for the dynamic weighting function are suggested in this context. Using a high-fidelity, moving-base driving simulation system, a human-in-the-loop pilot study was carried out, specifically recording ego vehicle motion data during lane changes. This data was utilized to calibrate the transitional IDM, demonstrating its efficacy in predicting the ego vehicle's longitudinal motion during lane changes. Furthermore, we compared the performance of various transitional functions and identified the hyperbolic tangent function as the most effective choice.

Copyright © 2024 The Authors. This is an open access article under the CC BY-NC-ND license (https://creativecommons.org/licenses/by-nc-nd/4.0/)

Keywords: Car-following model, intelligent driver model (IDM), lane changes, transitional function

1. INTRODUCTION

A. Background

Car-following models are pivotal for understanding how a vehicle longitudinally behaves as it trails another vehicle on the road (Wang et al., 2021). These models are essential tools in dissecting traffic dynamics and evaluating safe distances between vehicles, among other applications. They form the foundation of microscopic traffic flow modelling and simulation, making them indispensable for transportation researchers and engineers striving to improve transportation systems. In addition to their relevance in transportation research, car-following models have also proven beneficial in the development of autonomous and automated driving functions. Notably, they inspire the design of adaptive cruise control (ACC) (Wang et al., 2002, Treiber et al., 2000) as well as cooperative adaptive cruise control (CACC) systems (Derbel et al., 2013) for platooning. Compared to control theoretical approaches, the car-following-model-inspired ACC and CACC systems tend to be more human-centric as they aim to mimic the responses of human drivers.

Car-following models can generally be classified into two main categories: theory-based and data-driven. In the theory-based category, kino-dynamic models are prominent. For instance, the Gipps Model ensures safe following distances by calculating speeds based on a driver's braking and acceleration limits (Gipps *et al.*, 1981). Similarly, the Newell Model focuses on maintaining constant spacing to the lead vehicle (Newell *et al.*, 2002). Additionally, the Intelligent Driver Model (IDM)

(Treiber et al., 2000) stands out as a car-following model. It dynamically adjusts a vehicle's acceleration to maintain safe following distances while reflecting individual driving behaviors, energy consumption, and comfort (Shen et al., 2022, Ma et al., 2022a, Ma et al., 2022b, Wang et al., 2022b). The second category revolves around machine-learning-based techniques. These models utilize methods such as deep neural networks and/or reinforcement learning to adapt to various driving scenarios. For instance, Hart et al. (2024) exemplify this approach in their work.

B. Extensions of the Intelligent Driver Model

Among these car-following models, the IDM arguably holds the most significant influence on transportation research and the advancement of intelligent driving functions. However, despite its prominence, IDM does have its limitations. Thus, there are potential areas where IDM can be further improved and extended. One noteworthy endeavor focuses on addressing numerical issues within the IDM equation. Albeaik et al. (2022) elucidate that vehicle speeds can occasionally exhibit unrealistically negative values. To tackle this challenge, the authors propose solutions such as velocity projections and implementing deceleration limits. Additionally, Derbel et al. (2013) propose adjusting the gap term to mitigate the problem of inaccurately predicting collisions. This adaptation entails augmenting the minimum distance between vehicles, particularly at higher speeds. Another cluster of efforts aims to expand the operating range of IDM. This includes efforts such as incorporating human sensory inputs, like the driver's visual angle, to enhance the modeling of car-following behaviors on

winding roads, as investigated by Zhang et al. (2023). Additionally, Zong et al. (2021) extended IDM for multivehicle platoons to accommodate the velocities and accelerations of multiple vehicles. Moreover, Wang et al. (2022a) endeavored to generalize IDM to predict car-following behaviors during lane changes. They introduced a parameter, T_{LC} , representing the lane change time, which they argued was crucial for shaping a hyperbolic tangent transition function to model lane changes and ensure smooth IDM acceleration during this process.

C. Research Gaps

Several limitations in the study by Wang *et al.* (2022) have been identified. Methodologically, the sole reliance on T_{LC} , a temporal parameter, to characterize the lane-change transitional phase may be inadequate. To effectively capture the lane-changing transition, real-time information on the lateral position of the ego vehicle is necessary (Lee *et al.*, 2004). Solely relying on T_{LC} makes it challenging to accommodate the non-uniform temporal nature of lane changes and individual human variations. Another limitation lies in the model validation; Wang *et al.* (2022) preliminarily validated their model with simple numerical simulations, lacking real-world data and human-in-the-loop testing. This raises concerns regarding the soundness and potential applicability of the model in real-world scenarios.

D. Contributions and Paper Organization

To address these limitations, we develop a systematically modified IDM model capable of predicting the longitudinal motion of the ego vehicle concerning both leading vehicles in the current and target lanes, pre, post, and during the lane change. This transitional model incorporates a dynamic weighting function, which adjusts the relative importance of each of the two leading vehicles during integration based on the ego vehicle's lateral displacement during the lane-changing maneuver. Regarding validation, we employ a high-fidelity, moving-base, driving simulation system and conduct human-in-the-loop experiments to validate the proposed extension to IDM. We use the Parameterized Derivative-Free Optimization Solver (Zhou *et al.*, 2023) to fit the IDM parameter values based on our collected data due to its efficacy in nonlinear hyperparameter optimization problems.

The structure of the paper is as follows. Section II presents both the original IDM and the modified version that accounts for lane-change transitions, along with several candidate transitional functions. Section III outlines the experimental setup used for gathering car-following data to validate the models. In Section IV, the performance of the models is examined. Finally, Section V presents the selected model with the most effective transitional function and explores avenues for future research.

2. IDM CAR-FOLLOWING MODEL AND MODIFICATION

This section details the Intelligent Driver Model equation and introduces the proposed modification. The IDM produces a modeled acceleration that enables the ego vehicle to conduct a

desired car-following behavior while keeping a safe distance from the lead vehicle. It is calculated based on the current traffic scenario and five model parameters defined as: desired speed v_0 (on a free road with no lead vehicles, based on speed limit), time headway T, minimum gap s_0 (bumper-to-bumper distance between ego vehicle and lead vehicle), maximum acceleration a, and comfortable braking deceleration b. The equation is set up as:

$$a_{IDM} = a \left[1 - \left(\frac{v_e}{v_o} \right)^4 - \left(\frac{s_0 + v_e T + \frac{v_e \Delta v}{2\sqrt{ab}}}{x_l - x_e - L_l} \right)^2 \right]. \tag{1}$$

In (1), Δv denotes the velocity difference between the ego and lead vehicles, v_e represents the velocity of the ego vehicle, x_l and x_e are the longitudinal positions of the lead vehicle and ego vehicle, respectively, and L_l is the length of the lead vehicle. The expression $x_l - x_e - L_l$ represents the bumper-to-bumper spacing. For simplicity, all vehicles are assumed to be of equal length in this scenario, though future studies may adapt the model to accommodate varying vehicle lengths. Next, we will describe how we adapt the IDM based on these definitions.

To demonstrate our IDM longitudinal acceleration with the transitional variables during a lane change, we first present the IDM longitudinal acceleration equation before the lane-change maneuver and after the lane-change maneuver as follows.

$$a_{IDM, before LC} = a \left[1 - \left(\frac{v_e}{v_o} \right)^4 - \left(\frac{s_{bLC}^*}{x_o - x_e - L} \right)^2 \right].$$
 (2)

In (2), s_{bLC}^* represents the desired bumper-to-bumper distance before the lane change,

$$s_{bLC}^* = s_0 + v_e T + \frac{v_e |v_{bLC} - v_e|}{2\sqrt{ab}}.$$
 (3)

In (3), v_{bLC} and x_{bLC} represent the velocity and longitudinal position of the lead vehicle prior to the lane change, respectively. In addition, L is the length of the vehicle which as explained earlier is a constant. In a similar fashion, the IDM acceleration equation after the lane change is presented as.

$$a_{IDM, \ after \ LC} = a \left[1 - \left(\frac{v_e}{v_o} \right)^4 - \left(\frac{s_{aLC}^*}{x_{aLC} - x_e - L} \right)^2 \right].$$
 (4)

And the bumper-to-bumper distance after the lane change,

$$s_{aLC}^* = s_0 + v_e T + \frac{v_{ego} |v_{aLC} - v_{ego}|}{2\sqrt{ab}}.$$
 (5)

In (4) and (5), v_{aLC} and x_{aLC} represent the velocity and longitudinal position of the lead vehicle after the lane change, respectively. To combine equations (2) and (4), we utilize transitional functions to combine v_{bLC} and v_{aLC} into a single velocity v_{tr} , and x_{bLC} and x_{aLC} into a single longitudinal position x_{tr} . Therefore, our new IDM longitudinal acceleration equation with the transitional variables is presented as:

$$a_{IDM, during LC} = a \left[1 - \left(\frac{v_e}{v_o} \right)^4 - \left(\frac{s_{tr}^*}{x_{tr} - x_e - L} \right)^2 \right],$$
 (6)

$$s_{tr}^* = s_0 + v_e T + \frac{v_e |v_{tr} - v_e|}{2\sqrt{ab}}.$$
 (7)

We refer to (6) as T-IDM, the transitional IDM acceleration equation. In the next section, we will discuss how the transitional variables are obtained.

3. TRANSITIONAL FUNCTIONS

In this section, we discuss how the transitional functions to produce the T-IDM evolved. We introduce and discuss the four transitional functions to be examined. Each function depends on a transitional variable r, which ranges from 0 to 1 and represents how much of the lane change maneuver has been completed. It is calculated based on the lateral positions of the ego vehicle, the lead vehicle before the lane change, and the lead vehicle after the lane change as:

$$r(t) = \frac{y_e(t) - y_{bLC}(t)}{y_{aLC}(t) - y_{bLC}(t)}.$$
 (8)

In (8), y_e is the lateral position of the ego vehicle, y_{bLC} is the lateral position of the lead vehicle before the lane change, and y_{aLC} is the lateral position of the lead vehicle after the lane change. The transitional variable r is calculated at each time step. The plot of r varying against time in a lane-changing maneuver is shown in Figure 1.

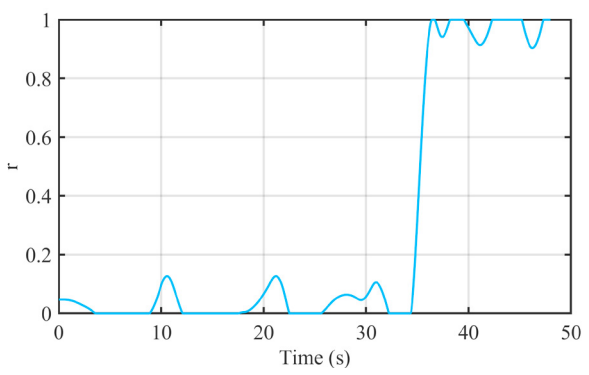


Figure 1. Variation of r against time.

Due to slight natural variations in human driving within a single lane, the variable r is constrained between 0 and 1. Future studies may incorporate a smoothing function to refine the lateral position deviations of the ego vehicle in traditional carfollowing scenarios. At r=0, the vehicle follows the classical IDM with the lead vehicle before the lane change, represented by $v_{tr}=v_{bLC}$ and $x_{tr}=x_{bLC}$. Conversely, at r=1, the scenario transitions to following the lead vehicle post-lane change, indicated by $v_{tr}=v_{aLC}$ and $x_{tra}=x_{aLC}$. In case there is no lead vehicle, a speed limit will be used. To illustrate these dynamics, we present plots of transitional functions ranging from 0 to 1. The first such function is linear, defined as:

$$\chi_{tr\,linear} = (1 - r)\chi_{bLC} + r \cdot \chi_{aLC},\tag{9}$$

where x can be replaced with v. The second transitional equation is a quadratic function of the form

$$x_{tr,quad} = (1 - r)^2 x_{bLC} + r^2 x_{aLC}.$$
 (10)

The third transitional equation is a hyperbolic tangent function of the form

$$x_{tr.tanh} = (1 - T(r))x_{bLC} + T(r)x_{aLC},$$
 (11)

$$T(r) = \frac{1}{2} \left(\tanh\left(f \cdot r - \frac{f}{2}\right) + 1\right),\tag{12}$$

where f is a tuning parameter. The fourth transitional equation is an exponential function of the form

$$x_{tr,exp} = (1 - E(r))x_{bLC} + E(r) \cdot x_{aLC},$$
 (13)

$$E(r) = \frac{e^{r^p} - 1}{e^1 - 1},\tag{14}$$

where p is a tuning parameter. The curves of these four transitional functions above, linear, quadratic, Eq. (12), and Eq. (14), are presented in Fig. 2.

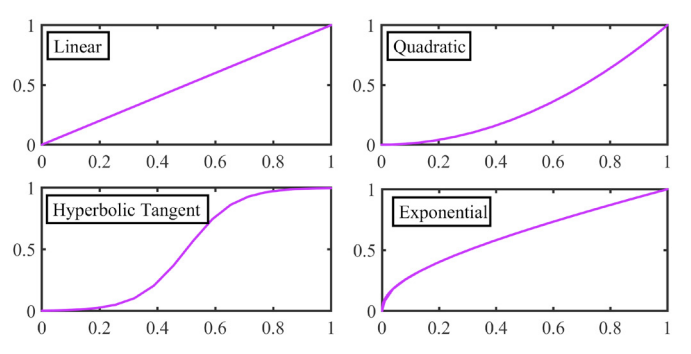


Figure 2. Curves of transitional functions to be used in T-IDM. The horizontal axis represents r values and the vertical axis represents transitional function output value.

Figure 2 demonstrates the smooth transition of functions from 0 to 1. Specifically, the hyperbolic tangent and exponential functions are parameterized with tuning constants f and r at 6 and 0.4 respectively. These settings confirm that at r=0.5, the functions indicate a lane change is half-complete. Future research could investigate the impact of parameter variations for more precise control. Notably, the exponential function's inherent asymmetry is particularly useful for differentiating lane change phases. Having integrated these functions into the reformed IDM equation, we will next assess their real-world efficacy using the T-IDM equation in a human-in-the-loop driving simulator experimentation.

4. EXPERIMENTAL DATA COLLECTION – DRIVING SIMULATOR AND SCENARIO DESCRIPTION

To collect real-world data for the thorough analysis of our T-IDM, we used a 6-degree-of-freedom (DoF) moving-base driving simulator (as shown in Figure 3) with one driver. The details of the simulator setup can be found in Zhou *et al.* (2023).



Figure 3. 6-DoF Moving-Base Driving Simulator.

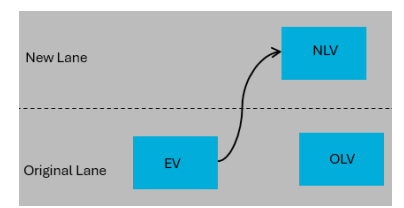


Figure 4. Highway scenario with ego vehicle (EV), original lead vehicle (OLV), and new lead vehicle (NLV).

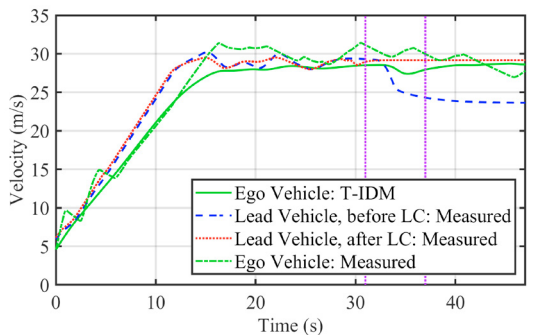


Figure 5. Linear transition T-IDM velocity (Scenario 1).

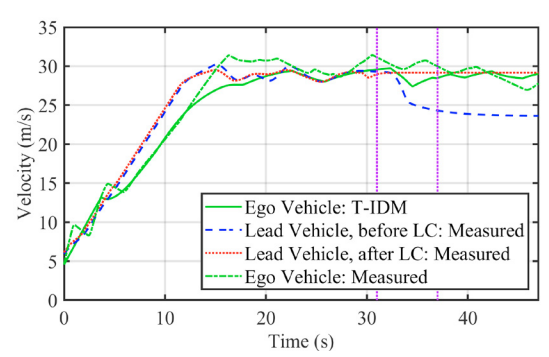


Figure 6. Quadratic transition T-IDM velocity (Scenario 1).

There are two scenarios in which data is collected as Figure 4 shows. In Scenario 1, two lead vehicles in separate lanes exhibit randomized speed variations to mimic natural driving conditions, maintaining an average speed of 28 m/s. The human driver initiates a lane change when the lead vehicle in the current lane starts braking, subsequently enabling both the ego and the target lane's lead vehicle to overtake the braking vehicle. In Scenario 2, the same conditions are applied except the lead vehicle in the target lane will suddenly slow down once the human driver of the ego vehicle initiates the lane change. As a result, the lead vehicle prior to the lane change overtakes both the ego vehicle and the new lead vehicle. We will now present the results of our model in these diverse scenarios.

5. MODEL PERFORMANCE

5.1 Results of Each Transitional Function

In this section, we present quantitative and qualitative comparisons of the models (with different transitional functions) in both scenarios. From Figures 5 - 12, the purple dotted line represents the start and end of the lane change. Upon analyzing velocity curves in Figures 5-8, we observed that the ego vehicle employing T-IDM decelerates and then accelerates around the 31-second mark during the lane change, initially due to the decelerating lead vehicle and subsequently transitioning to match the higher speed of the new lead vehicle at r=0.5.

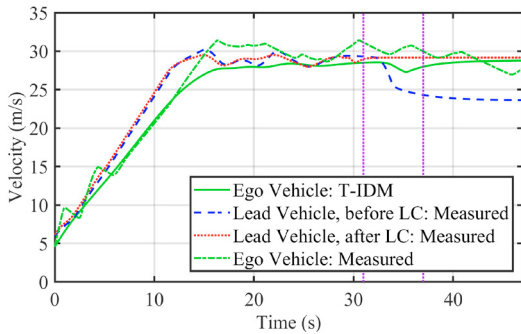


Figure 7. Hyperbolic tangent transition T-IDM velocity (Scenario 1).

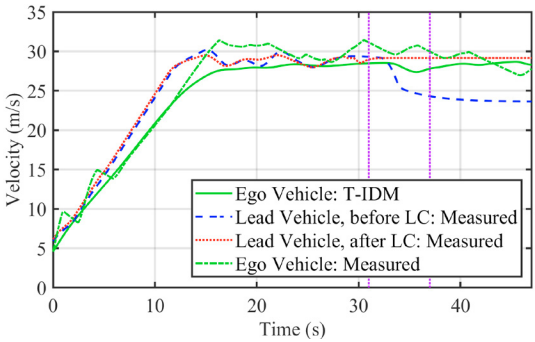


Figure 8. Exponential transition T-IDM velocity (Scenario 1).

On the other hand, Scenario 2 offers additional insights. The velocity curves in Figures 9-12 show a sudden deceleration of the new lead vehicle, with the ego vehicle demonstrating slower velocity adaptation compared to Scenario 1. Nevertheless, the T-IDM effectively prevents overtaking in most transitions, maintaining close velocity alignment.

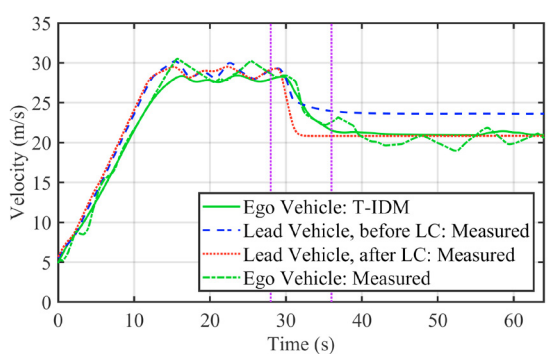


Figure 9. Linear transition T-IDM velocity (Scenario 2).

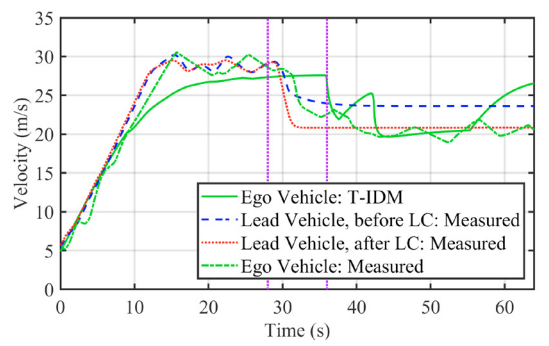


Figure 10. Quadratic transition T-IDM velocity (Scenario 2).

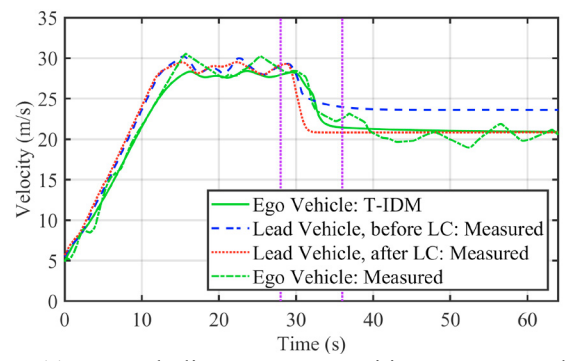


Figure 11. Hyperbolic tangent transition T-IDM velocity (Scenario 2).

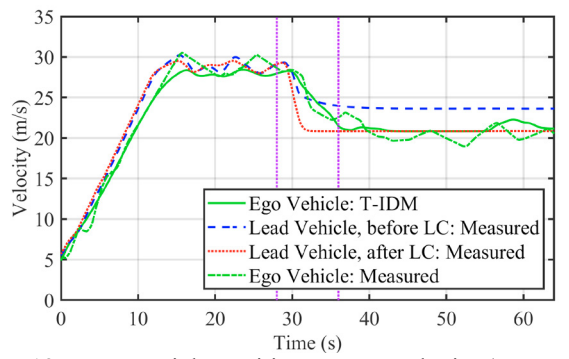


Figure 12. Exponential transition T-IDM velocity (Scenario 2).

5.2 Analysis and Comparison of the Transitional Functions

In this section, we present a detailed analysis of transitional functions within the T-IDM. The quadratic transition, with its sharp curvature, is dismissed due to its pronounced jerk in Figure 10. Additionally, as illustrated in Figure 2, the exponential function doesn't exhibit tapering as r approaches 0 and 1, and its steep slope in this range heightens sensitivity to fluctuations in r, leading to unstable T-IDM velocities. As a result, the exponential function shows significant velocity variance after the lane change, highlighting its instability due to a steep slope at the extremes of r, as seen in Figures 8 and 12. Conversely, the hyperbolic tangent function demonstrates superior performance in vehicle speed management during lane changes, as shown by smoother transitions in Figures 7 and 11. It ensures stable car-following behavior and outperforms the linear transition. Notably, despite the speed being slightly greater post-lane change in Figure 11, the longitudinal position curve in Figure 13 confirms that the ego vehicle maintains effective car-following behavior with the new lead vehicle, contrasting with the quadratic transition where the T-IDM ego vehicle overtakes the new lead vehicle. Supported by qualitative data and root-mean-squred-error (RMSE) metrics, the hyperbolic tangent function is confirmed as the most effective for adapting to new lead vehicle velocities in the T-IDM model.

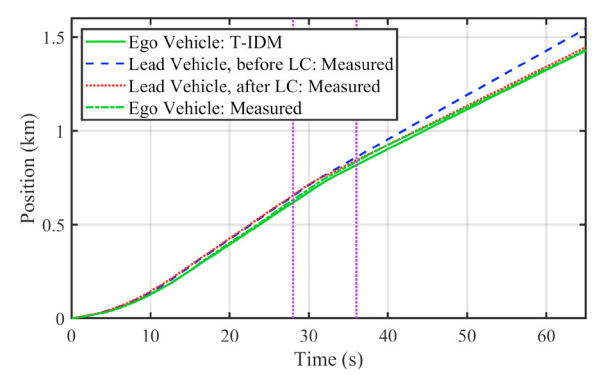


Figure 13. Hyperbolic tangent transition T-IDM longitudinal position (Scenario 2).

In Tables 1 and 2, we evaluated the RMSE values between the T-IDM-calibrated and the measured velocities of the ego vehicle during lane changes with different transitional functions. Scenario 1 exhibits higher RMSE values due to a significant slowdown by a lead vehicle, while Scenario 2 provided consistent slowing from all vehicles. The quadratic transition yielded the highest RMSE, with linear transition performing best during, but not after, the lane change. The hyperbolic tangent transition demonstrated reasonable RMSE values, supporting its selection.

Table 1. RMSE of T-IDM ego vehicle velocity and measured ego vehicle velocity during the lane change (Scenario 1).

Linear	Quadratic	Hyperbolic	Exponential
RMSE	RMSE	Tangent RMSE	RMSE
2.3220	1.8138	2.3135	2.3330

Table 2. RMSE of T-IDM ego vehicle velocity and measured ego vehicle velocity during the lane change (Scenario 2).

Linear	Quadratic	Hyperbolic	Exponential
RMSE	RMSE	Tangent RMSE	RMSE
0.5507	3.3771	0.7026	0.8015

6. CONCLUSIONS AND FUTURE WORK

In this paper, we explored a novel transitional Intelligent Driver Model (T-IDM) designed for performing car-following during lane-change maneuvers involving two lead vehicles (one in each lane) with variable speeds. Our findings indicate that the hyperbolic tangent transitional function facilitates the smoothest car-following behavior during and after a lane change. The introduction of a new transition parameter r significantly enhances the T-IDM's ability to smoothly shift car-following from the original to the target lead vehicle as it accounts for human behavior. Despite the success, further validation of this model is necessary using real-world datasets

such as NGSIM and highD. Future work could also explore using smoothing techniques for the transition parameter to mitigate the inherent lateral position variability caused by human driving behaviors. Additionally, we may want to investigate defining the transition parameter with some objective measurements.

ACKNOWLEDGEMENT

This work was partially supported by NSF Awards 2312465 and 2312466.

REFERENCES

- Albeaik, S., Bayen, A., Chiri, M. T., Gong, X., Hayat, A., Kardous, N., Keimer, A., McQuade, S. T., Piccoli, B., & You, Y. (2022). Limitations and improvements of the intelligent driver model (Idm). SIAM Journal on Applied Dynamical Systems, 21(3), 1862–1892. https://doi.org/10.1137/21M1406477
- Ciuffo, B., Makridis, M., Toledo, T., & Fontaras, G. (2018).

 Capability of current car-following models to reproduce vehicle free-flow acceleration dynamics. *IEEE Transactions on Intelligent Transportation Systems*, 19(11), 3594–3603. https://doi.org/10.1109/TITS.2018.2866271
- Derbel, O., Peter, T., Zebiri, H., Mourllion, B., & Basset, M. (2013). Modified Intelligent Driver Model for driver safety and traffic stability improvement. *IFAC Proceedings Volumes*, 46(21), 744–749. https://doi.org/10.3182/20130904-4-JP-2042.00132
- Gipps, P. G. (1981). A behavioural car-following model for computer simulation. *Transportation Research Part B: Methodological*, 15(2), 105–111. https://doi.org/10.1016/0191-2615(81)90037-0
- Hart, F., Okhrin, O., & Treiber, M. (2024). Towards robust carfollowing based on deep reinforcement learning. *Transportation Research Part C: Emerging Technologies*, 159, 104486. https://doi.org/10.1016/j.trc.2024.104486
- Kesting, A., Treiber, M., & Helbing, D. (2010). Enhanced intelligent driver model to access the impact of driving strategies on traffic capacity. *Philosophical Transactions of the Royal Society A: Mathematical, Physical and Engineering Sciences*, 368(1928), 4585–4605. https://doi.org/10.1098/rsta.2010.0084
- Ma, Y. and Wang, J. (2022). Personalized Driving Behaviors and Fuel Economy over Realistic Commute Traffic: Modeling, Correlation, and Prediction, *IEEE Transactions* on Vehicular Technology, 71(7), 7084-7094, https://doi.org/10.1109/TVT.2022.3171165
- Ma, Y. and Wang, J. (2022). Energetic Impacts Evaluation of Eco-Driving on Mixed Traffic with Driver Behavioral Diversity, *IEEE Transactions on Intelligent Transportation Systems*, 23(4), 3406-3417, 2022, https://doi.10.1109/TITS.2020.3036326
- Newell, G. F. (2002). A simplified car-following theory: A lower order model. *Transportation Research Part B: Methodological*, 36(3), 195–205. https://doi.org/10.1016/S0191-2615(00)00044-8

- Rothery, R. W. (1992). *Car following models*. Traffic Flow Theory: A State-of-the-Art Report, Revised Monograph on Traffic Flow Theory.
- S. E. Lee, E. C. B. Olsen, and W. W. Wierwille, "A Comprehensive Examination of Naturalistic Lane-Changes," DOT HS 809 702, *Virginia Tech Transportation Institute*, Blacksburg, VA, March 2004.
- Shen, H., Wang, Z., Zhou, X., Lamantia, M., Yang, K., Chen, P., & Wang, J. (2022). Electric vehicle velocity and energy consumption predictions using transformer and markovchain monte carlo. *IEEE Transactions on Transportation Electrification*, 8(3), 3836–3847. https://doi.org/10.1109/TTE.2022.3157652
- Treiber, M., Hennecke, A., & Helbing, D. (2000). Congested traffic states in empirical observations and microscopic simulations. *Physical Review E*, 62(2), 1805–1824. https://doi.org/10.1103/PhysRevE.62.1805
- T. T. Zhang, P. J. Jin, S. T. McQuade, A. Bayen, and B. Piccoli, "Car-Following Models: A Multidisciplinary Review," *arXiv*:2304.07143v4 [eess.SY], Mar. 5, 2024.
- Wang, J. and Rajamani, R. (2002). Adaptive Cruise Control System Design and Its Impact on Traffic Flow, *American Control Conference*, pp. 3690 3695. https://doi.org/10.1109/ACC.2002.1024501
- Wang, Y., Cao, X., & Ma, X. (2022). Evaluation of automatic lane-change model based on vehicle cluster generalized dynamic system. *Automotive Innovation*, *5*(1), 91–104. https://doi.org/10.1007/s42154-021-00171-z
- Wang, Z., Zhou, X., & Wang, J. (2021). Algebraic carfollowing model parameter identification. *IFAC-PapersOnLine*, 54(20), 864–869. https://doi.org/10.1016/j.ifacol.2021.11.280
- Wang, Z., Zhou, X., & Wang, J. (2022). An algebraic evaluation framework for a class of car-following models. *IEEE Transactions on Intelligent Transportation Systems*, 23(8), 12366–12376. https://doi.org/10.1109/TITS.2021.3113788
- Zhang, X., Shi, Z., Yu, S., & Ma, L. (2023). A new carfollowing model considering driver's desired visual angle on sharp curves. *Physica A: Statistical Mechanics and Its Applications*, *615*, 128551. https://doi.org/10.1016/j.physa.2023.128551
- Zhou, X., Wang, Z., Cosio, A., & Wang, J. (2021). Parameterized derivative-free optimization approach for car-following model calibration. *IFAC-PapersOnLine*, 54(20), 876–881.

https://doi.org/10.1016/j.ifacol.2021.11.282

- Zhou, X et al. (2023). A novel instrumental system for immersive simulation-based driver-in-the-loop vehicular technology research and validation. 2023 IEEE International Automated Vehicle Validation Conference (IAVVC), 1–6. https://doi.org/10.1109/IAVVC57316.2023.10328070
- Zong, F., Wang, M., Tang, M., Li, X., & Zeng, M. (2021). An improved intelligent driver model considering the information of multiple front and rear vehicles. *IEEE Access*, 9, 66241–66252. https://doi.org/10.1109/ACCESS.2021.3072058